Title: Linking mechanistic analysis of catalytic reactivity cliffs to ligand classification

Authors: Samuel H. Newman-Stonebraker[1†], Sleight R. Smith[2†], Julia E. Borowski[1], Ellyn Peters[2], Tobias Gensch[2], Heather C. Johnson[3], Matthew S. Sigman[2]*, Abigail G. Doyle[1]*

Affiliations:

[1]Department of Chemistry, Princeton University, Princeton, NJ 08544.

[2]Department of Chemistry, University of Utah, Salt Lake City, UT 84112.

[3]Process Research and Development, Merck & Co., Inc., Rahway, NJ 07065

*Corresponding author. Email: sigman@chem.utah.edu (M.S.S.), agdoyle@princeton.edu (A.G.D.)

[†]*These authors contributed equally*

Abstract: Statistical analysis of reaction data with molecular descriptors can enable chemists to identify reactivity cliffs that result from a mechanistic dependence on a specific structural feature. In this study, we develop a broadly applicable and quantitative classification workflow that identifies reactivity cliffs in eleven Ni- and Pd-catalyzed cross-coupling datasets employing monodentate phosphine ligands. A unique ligand steric descriptor, $\%V_{bur}$ (*min*), is found to divide these datasets into active and inactive regions at a similar threshold value. Organometallic studies demonstrate that this threshold corresponds to the binary outcome of bisligated versus monoligated metal and that $\%V_{bur}$ (*min*) is a physically meaningful and predictive representation of ligand structure in catalysis. Taken together, we expect that this strategy will be of broad value in mechanistic investigation of structure-reactivity relationships, while providing a means to rationally partition datasets for data-driven modeling.

Main text:

For almost 100 years, chemists have used data-driven modeling to understand the many complex relationships connecting chemical structure to reactivity. The paradigmatic example is the

Hammett equation (*1*), a linear free energy relationship (LFER) between an experimental observable and a molecular descriptor (*2*). LFERs have been used extensively to understand reaction mechanism (*3, 4*) and, in certain cases, to predict reaction outcomes (*5*). While many reactions are continuously dependent on a single descriptor, as captured by LFERs, some processes may exhibit reactivity cliffs, wherein a criterion or threshold value of a given feature must be met in order for the reaction to occur (i.e., a binary response) (*6*). If a particular molecular feature can define a reactivity cliff and classify molecules by structure, this could be used to predict reaction performance of unseen examples while also resulting in the development of key mechanistic insights (**Fig. 1A**). Thus, the identification and understanding of these reactivity cliffs is of great interest, as the ability to bifurcate datasets—and the molecules within them—on the basis of distinct mechanistic outcomes would augment expert chemists' intuition and simplify subsequent data-driven modeling.

Transition metal-catalyzed cross coupling represents an interesting case study for identifying reactivity cliffs. This reaction class is synthetically important due to its widespread use in the construction of pharmaceuticals (*7*) and materials (*8*). In addition, the success of these reactions is highly dependent on ligand identity, for which monodentate phosphines are ubiquitous (*9, 10*). As a result, chemists have developed numerous tools to quantitatively describe the diverse steric and electronic properties of these ligands—for which thousands of unique structures exist—to uncover structure-reactivity relationships (SRRs) in experimental data (*11*) (**Fig. 1B**). These descriptors, including Tolman Cone Angle (*12, 13*), Solid Angle (*14*), Sterimol (*15*), and percent buried volume (%V_{bur}) (*16, 17*), have been used successfully in linear modeling of cross-coupling reactions (*5, 18*) (**Fig. 1C**). However, there are situations in which seemingly similar ligands afford

substantially different responses (*19*), suggesting the presence of discontinuous trends in ligand activity (*20*).

Considering this, we hypothesized that reactivity cliffs were embedded in a phosphine structural feature that had yet to be recognized. Identification of such a feature would not only allow for the development of a statistical tool to classify active and inactive ligands but also provide a quantitative handle for mechanistically rationalizing ligand performance. Herein we provide a workflow and analysis to achieve these goals. Using the organophosphorus(III) descriptor library recently developed by Sigman and Aspuru-Guzik (*Kraken*) that possesses over 190 conformationally representative descriptors for each of several thousand monodentate phosphines (*21*) (**Fig. 1D**), we were able to classify eleven Ni and Pd catalytic case studies into mechanistically bifurcated regions of reactivity based on catalyst ligation state, consistent with spectroscopic/crystallographic organometallic studies. We found that minimum percent buried volume (%V_{bur} (*min*))—a previously unexplored descriptor that quantifies the proximal steric bulk of the smallest energetically accessible conformation of a given ligand—is the single descriptor able to achieve this classification. Ultimately, we demonstrate that this analysis was able to reveal non-intuitive trends in organometallic chemistry and thereby serves as an important mechanistic tool, complementary to LFERs (*18, 19*), to understand and predict monodentate phosphine SRRs and catalyst speciation in cross-coupling catalysis (**Fig. 1E**).

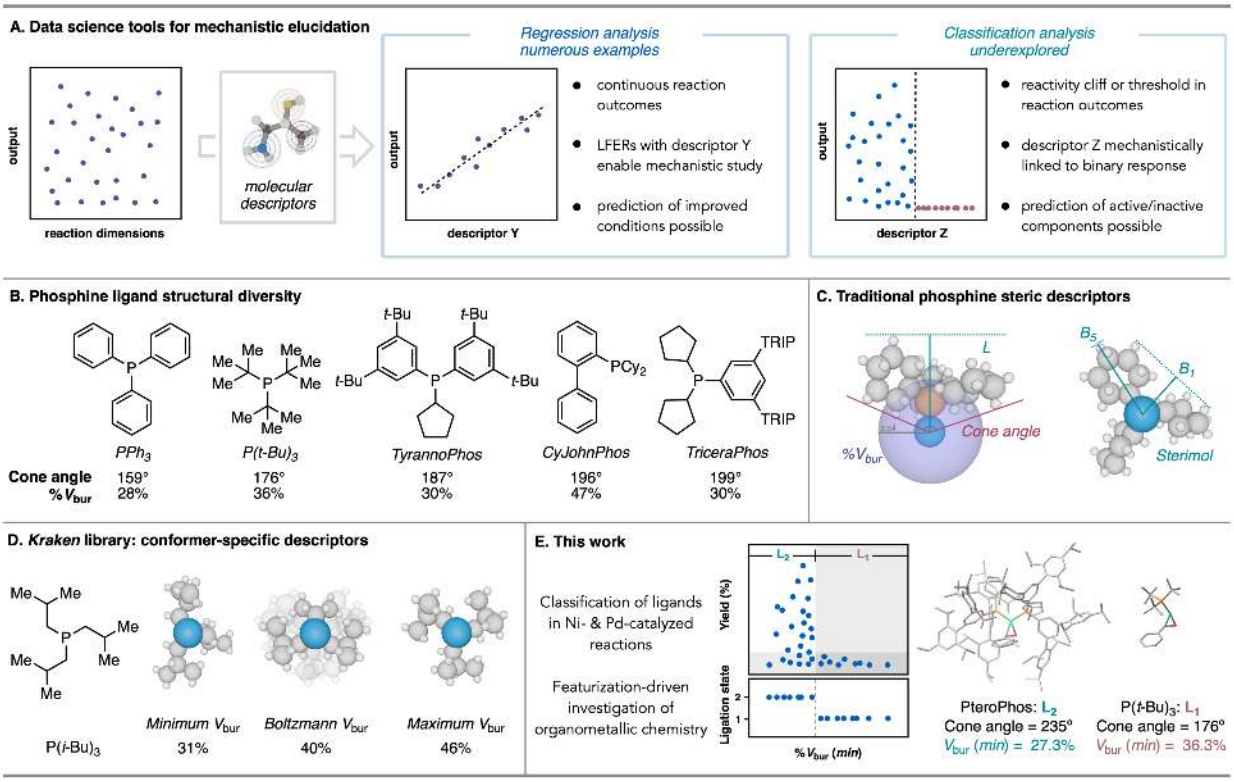

Fig. 1. Introduction. (**A**) Tools to understand trends in chemical reactivity using mechanistically relevant molecular descriptors. (**B**) Examples of monodentate phosphines used in Ni and Pd cross-coupling reactions, including TyrannoPhos and TriceraPhos (DinoPhos ligands) recently reported by the Doyle lab. TRIP = 2,4,6-triisopropylphenyl. (**C**) Commonly employed methods of quantifying phosphine steric properties. (**D**) Phosphine descriptor library (*Kraken*) capturing multiple ligand conformers. (**E**) This work.

Results and Discussion

Exploration of phosphine steric features in Ni-catalysis.

Our initial platform for probing the presence of ligand reactivity cliffs was inspired by a recent study from the Doyle group that identified a new class of phosphine ligands—the DinoPhos ligands (TriceraPhos and TyrannoPhos (**Fig. 1B**))—for Ni-catalyzed cross-coupling of acetals with aryl boroxines (*19*). Having both large cone angles and small %V_{bur} values, these ligands are distinct from other phosphines that often have a 1:1 relationship between these features (*22*). The large cone angles suggested that the DinoPhos ligands may behave like the sterically bulky phosphines developed for Pd catalysis (e.g., P(*t*-Bu)$_3$ or BrettPhos), where formation of

monoligated Pd (L_1 complexes) has been shown to be critical for reaction success (*23*-*27*). However, the small $\%V_{bur}$ characterized these ligands as similar to smaller structures (e.g., PPh_3) that tend to form bisligating (denoted as L_2) complexes. The observation that this unique steric profile was essential for reaction success in Ni catalysis raised questions about its impact on speciation and prompted us to use Ni-catalyzed cross-coupling reactions as a case study for the identification of ligand reactivity cliffs.

The original study by the Doyle lab included 19 phosphines, which we supplemented with 15 additional ligands to span the entire range of $\%V_{bur}$ (**I**, Figure 2A). We also collected data on more traditional Csp^2–Csp^2 Suzuki–Miyaura coupling reactions with aryl chlorides using high-throughput experimentation (HTE) (*28*). The ligand set was selected from a combined Doyle and Merck inventory to encompass 90 monodentate ligands that are evenly distributed throughout the feature space from the Sigman/Aspuru-Guzuk virtual library (*21*) as determined by principal component analysis. These ligands were evaluated for four cross-coupling reactions wherein the aryl halide and aryl boronic acid were altered (**II**-**V**, Figure 2A). The coupling partners included a range of electronic and steric features that could impact different aspects of the elementary steps of the catalytic cycle. Notably, the DinoPhos ligands were top performers in each of these reactions, along with DrewPhos (*29*), a triarylphosphine ligand that possesses large 3,5-substituents similar to the DinoPhos ligands.

With these data, we sought to determine how the recently computed phosphine steric descriptors relate to reaction performance. For each reaction, the yield was evaluated against representative descriptors in the library; as three examples, the cone angle (*30*), Boltzmann averaged $\%V_{bur}$ of the ligand's conformational ensemble ($\%V_{bur}$ (*Boltz*)), and $\%V_{bur}$ of the library conformer with the smallest buried volume ($\%V_{bur}$ (*min*)) are shown in Figure 2B. While the cone

angle descriptors did not provide clear reactivity cutoffs, both %V_{bur} (*Boltz*) and %V_{bur} (*min*) allowed for visual classification of ligand performance into "active" and "inactive" bins (details of the classification tool will be described below), though several outliers were present with the former. %V_{bur} (*min*) revealed sharp cutoffs in reactivity, wherein nearly all ligands above 32% were found to be unreactive. Ligands that were unsuccessful at promoting reactivity below 32% V_{bur} (*min*) were grouped in their own bin, wherein electronic features and catalyst-poisoning functionality (e.g., cyano, carbonyl, and halide groups) appeared to be largely responsible for their inactivity. Notably, the use of %V_{bur} (*min*) but not %V_{bur} (*Boltz*) allowed for various highly-flexible scaffolds such as P(*i*-Bu)$_3$, PBn$_3$, and small Buchwald-type phosphines (*31, 32*), to be successfully classified. Thus, this steric descriptor was best able to categorize phosphines into active and inactive groups, with a reactivity threshold of ~32% V_{bur} (*min*) appearing to be largely independent of the substrate pairing.

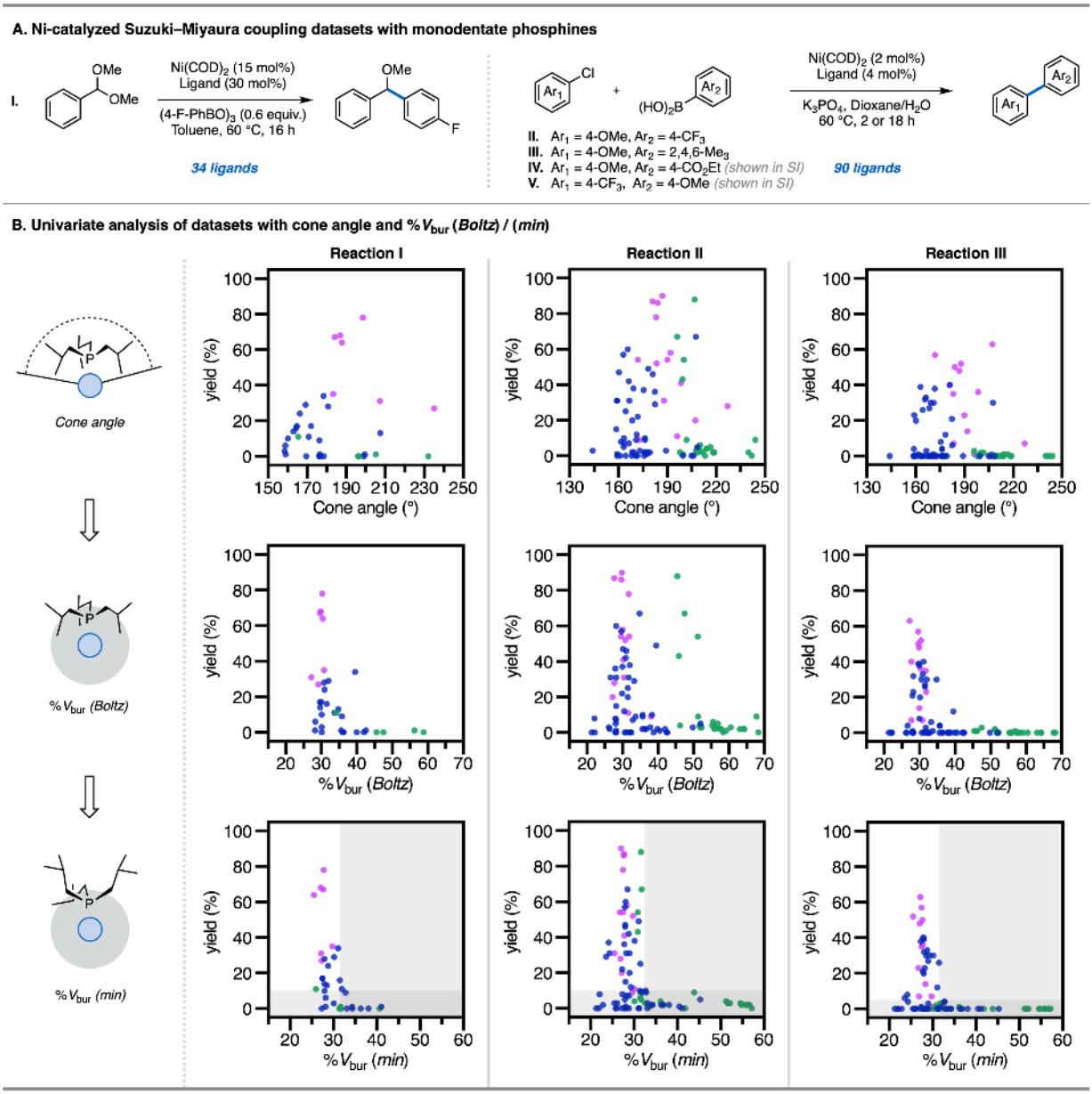

Fig. 2. Investigation of phosphine steric parameters in Ni catalyzed datasets. (**A**) Ni-Catalyzed Suzuki-Miyaura datasets collected with monodentate phosphine ligands, including the DinoPhos ligands. (**B**) Analysis of datasets with steric parameters cone angle, %V_{bur} Boltz. and %V_{bur} min.. Pink dots = DinoPhos-type ligands, green dots = Buchwald-type ligands, blue dots = all others.

Mechanistic origin of %V_{bur} (min) reactivity thresholds. The presence of reaction-independent reactivity cliffs relative to %V_{bur} (*min*) in these data prompted us to investigate the mechanistic basis for this descriptor's significance. Given the importance of speciation in cross-coupling catalysis, we questioned whether this descriptor is predictive of the thermodynamic favorability of

L_2M vs. L_1M speciation. Historically, the development of large ligands—intuitively captured through the cone angle descriptor—is an established principle to encourage L_1M and achieve reactivity in Pd catalysis (*23-27*). While TriceraPhos and TyrannoPhos both have cone angle values higher than many phosphines known to form L_1 species, $\%V_{bur}$ (*min*) categorizes their reactivity with those that form L_2 Ni and Pd complexes (*23, 33*). Thus, this interpretation of the observed reactivity cliffs would suggest that steric bulk within the metal's first coordination sphere primarily governs the ligation state outcome, regardless of the overall size of the phosphine.

To interrogate this hypothesis, we surveyed a subset (28 phosphines) of the ligands used across the Ni-catalyzed SMC reactions to determine ligation state spectroscopically. L_nNi(4-fluorobenzaldehyde) was chosen as a platform, as its three NMR handles (^1H, ^{19}F, and ^{31}P) provided a readout of the *in-situ* ligation state at the metal center upon reaction of $Ni(COD)_2$ with the aldehyde and two equivalents of phosphine (**VI**, Figure 3A) (*34, 35*). Each ligand was assigned as forming L_2Ni or L_1Ni complexes based on the observed spectra. The results of these experiments were then evaluated with steric features from the library to determine which classified the ligands into regions of similar ligation states (Figure 3B, see SI for additional parameters). As observed with the cross-coupling reaction yields, cone angle was unable to partition the ligands. Indeed, the DinoPhos ligands and DrewPhos all formed L_2Ni complexes exclusively, despite having some of the largest cone angle values among ligands evaluated. $\%V_{bur}$ (*Boltz*) was able to correctly group the DinoPhos-type ligands with other L_2Ni-forming phosphines; however, some flexible ligands

(MeJohnPhos, P(*i*-Bu)$_3$, and PBn$_3$) remained misclassified with L$_1$Ni-forming ligands. Similar to the catalytic reactions, %V_{bur} (*min*) resolved these outliers and resulted in a sharp cutoff just below 32% between the L$_2$Ni and L$_1$Ni regimes. Notably, this value closely matched the reactivity thresholds observed in reactions **I**-**V**.

Given this finding, we hypothesized that one could predict the speciation of new ligands, enabling a pre-screening of structures that may be challenging to access synthetically. To test this, we conceptualized a new DinoPhos ligand, PteroPhos, which possesses two aryl groups with 2,4,6-triisopropylphenyl (TRIP) substituents at the 3,5-positions (Figure 4A). Its computed cone angle is 235º, one of the largest among all monodentate phosphines studied. Despite the enormous size of this ligand as ascertained by visual inspection and its cone angle value, its relatively low %V_{bur} (*min*) of only 27.2% suggested that PteroPhos should form L$_2$Ni complexes and be effective in Ni-catalyzed SMCs. Indeed, upon preparation of this

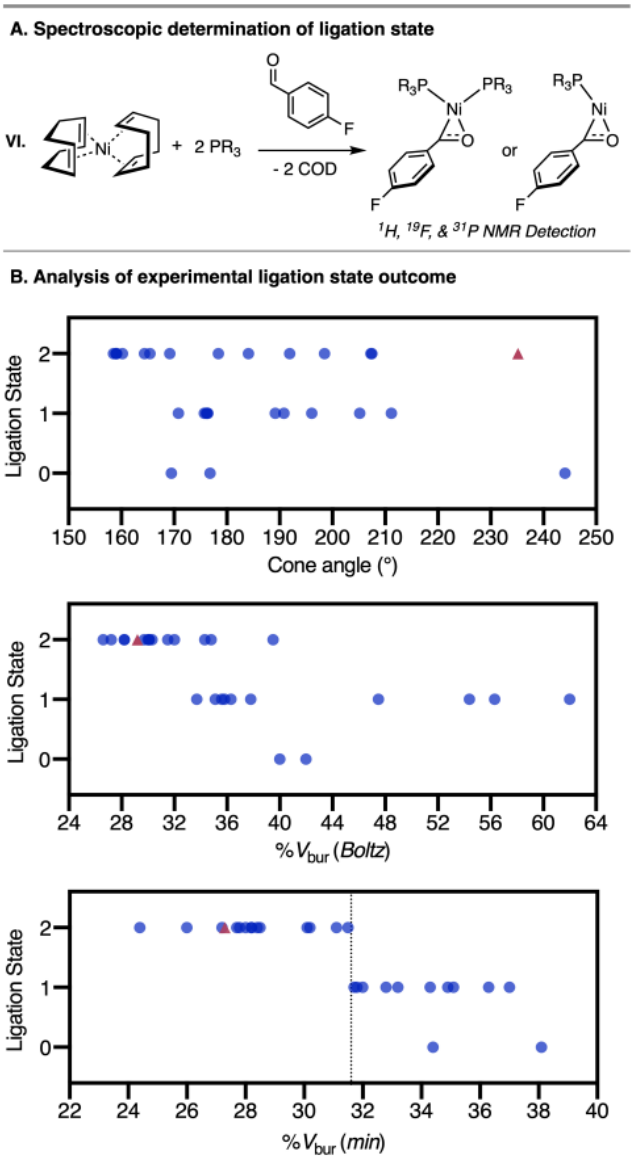

Fig. 3. Ligation state studies. (**A**) Reaction of Ni(COD)$_2$, 4-fluorobenzaldehyde, and 2 equivalents of phosphine for spectroscopic determination of ligation state using ^{1}H, ^{19}F, and ^{31}P NMR spectroscopy in C$_6$D$_6$ (25 °C). (**B**) Ligation state experiments plotted against cone angle, %V_{bur} (*Boltz*), and %V_{bur} (*min*). Red triangle represents PteroPhos. (*t*-Bu)BrettPhos (non-ligating) datapoint beyond x-axis range for %V_{bur} (*min*)/(*Boltz*) plots.

ligand, we found that it readily formed a L_2Ni(4-fluorobenzaldehyde) complex (Figure 3B) and was moderately active in Ni-catalyzed reactions **I-V**, consistent with the $\%V_{bur}$ (*min*) classification analysis.

We then sought to understand the structural significance of $\%V_{bur}$ (*min*) through crystallographic and computational studies (complexes **1**-**4**, Figure 4A), first to rationalize why cone angle is not predictive of speciation. While our attempts at crystallizing L_2Ni(benzaldehyde) complexes bearing the DinoPhos ligands were not successful, we were able to obtain X-ray quality crystals of (DrewPhos)$_2$Ni(2-naphthaldehyde) (**3**, Figure 4A). As observed in the solid state, the two phosphines are positioned 116º *cis* to each other on the complex; since DrewPhos possesses a cone angle of 207º, a literal interpretation of cone angle as a description of phosphine size would suggest that there is 90º overlap of two solids, giving rise to considerable steric repulsion or distortion. Yet, when compared with the X-ray structure of (PPh_3)$_2$Ni(2-naphthaldehyde) (**1**, Figure 4A), the two complexes exhibit very similar Ni–P bond lengths and P–Ni–P "bite angles", despite DrewPhos having a cone angle 48º larger than PPh_3. What cone angle does not capture is the non-uniform topology of the ligand structure distal to the metal. These less dense and more conformationally flexible regions can be arranged in a manner that accommodates a second ligand and/or substrate within the "cone", a recognized limitation that has led to the development of alternative steric parameters (*16, 36*). On this basis, cone angle is unsuccessful at classifying the ligation state and reactivity of the phosphines under study. Indeed, when compared with that of L_1 (P(*t*-Bu)$_3$)Ni(benzaldehyde) (**2**) (Figure 4A), the DFT-optimized structure of (PteroPhos)$_2$Ni(benzaldehyde) (**4**) (Figure 4A) provides the most striking example of L_2 complexation being agnostic to substantial remote steric bulk.

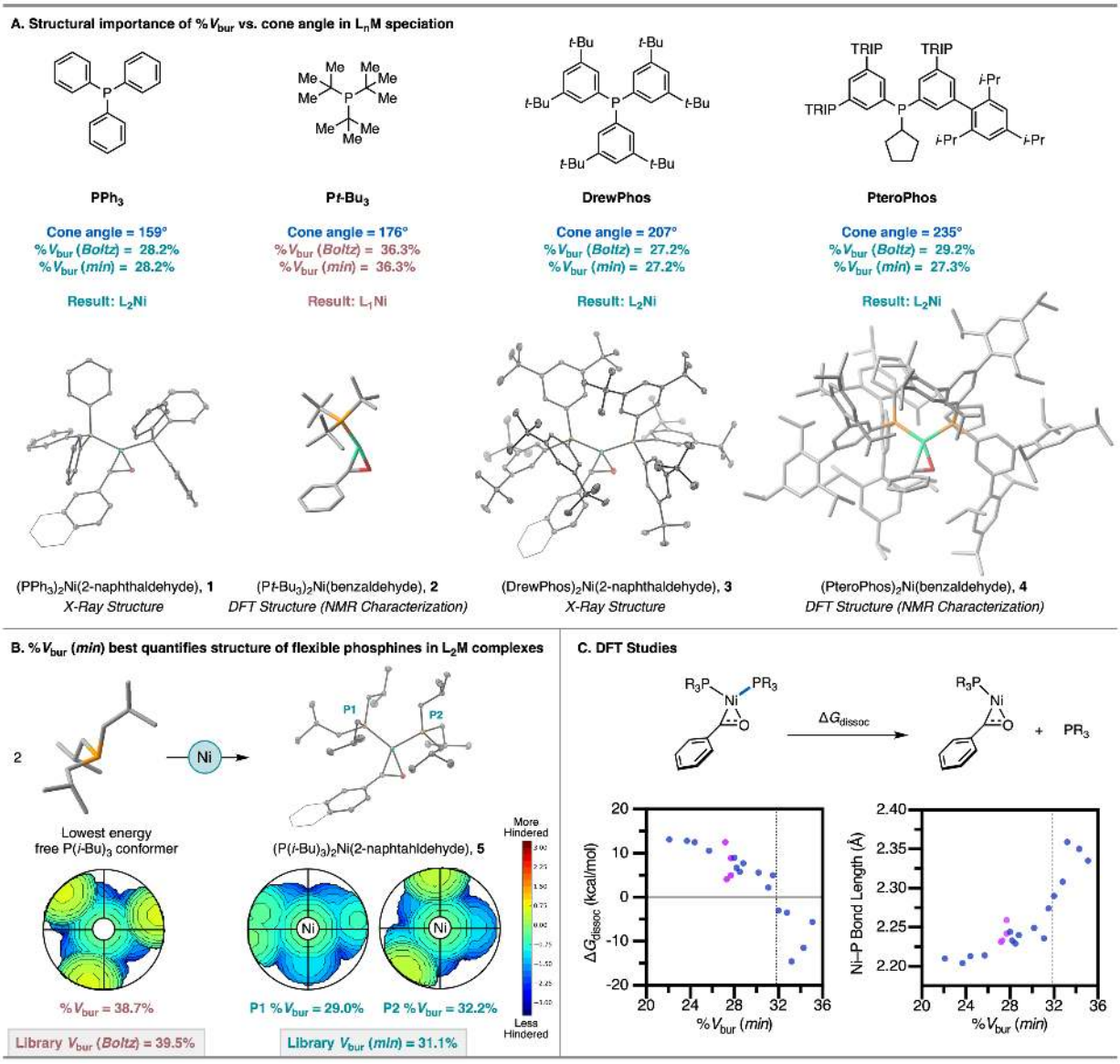

192

193 **Fig. 4. Mechanistic studies of %V_{bur} (*min*) ligation state threshold**. (**A**) Ligands with large cone angles
194 but relatively small %V_{bur} values can form L_2Ni, supported structurally by solid-state structures of
195 $(PPh_3)_2Ni$(2-naphthaldehyde)[a] and $(DrewPhos)_2Ni$(2-naphthaldehyde)[a], along with DFT structures of (P(*t*-
196 Bu)$_3$)Ni(benzaldehyde) and $(PteroPhos)_2Ni$(benzaldehyde) optimized at the B3LYP-D3/6-31G(d,p)[SDD]
197 level of theory. (**B**) Formation of $(P(i\text{-}Bu)_3)_2Ni$(2-naphthaldehyde)[a], with %V_{bur} values of the ligands bound
198 are in agreement with the library value of %V_{bur} (*min*) (**C**) DFT calculated dissociation energies and bond
199 lengths for L_2Ni(benzaldehyde) complexes. Ni–P bond length calculated from highlighted bond. DinoPhos-
200 type ligands (including DrewPhos) highlighted in purple. Calculations performed at M11-L/def2-
201 TZVP|SMD(benzene)//B3LYP-D3/6-31G(d,p)[SDD]|SMD(benzene) level of theory. [a](ORTEP diagram
202 with 30% thermal ellipsoids shown. Hydrogens omitted for clarity).

203 While this case study highlights the dependence of speciation on steric bulk within the first

204 coordination sphere, which is captured by the %V_{bur} parameters, the ligands investigated in Fig.

4A had small variations between their %V_{bur} (*min*) and %V_{bur} (*Boltz*) values. To better understand the structural importance of %V_{bur} (*min*) in the classification of the catalytic (Figure 2B) and ligation state experiments (Figure 3B), the L_2Ni-forming ligand with the greatest difference between %V_{bur} (*min*) and %V_{bur} (*Boltz*) values, P(*i*-Bu)$_3$, was investigated. For this phosphine, lowest energy conformer and Boltzmann average %V_{bur} values (38.7% and 39.5%, respectively) are both substantially higher than other L_2Ni-forming ligands, and even higher than that of L_1Ni-forming P(*t*-Bu)$_3$ (36.3%). However, an X-ray crystal structure of (P(*i*-Bu)$_3$)$_2$Ni(2-naphthaldehyde) (**5**) (Figure 4B) confirmed that two phosphines were bound to Ni, with %V_{bur} values determined to be 29.0% and 32.2%, nearly matching that of %V_{bur} (*min*) (31.1%). Thus, only %V_{bur} (*min*), which was designed to capture the degree of conformational flexibility, simulates the redistribution of steric bulk out of the metal's first coordination sphere in order to accommodate both ligands and the substrate for phosphines like P(*i*-Bu)$_3$.

Finally, given the sharp catalytic and ligation state reactivity cliffs, we postulated that there would be a strong dependence on the thermodynamics of phosphine dissociation with %V_{bur} (*min*). Out of all 28 phosphines studied in Figure 3, only one (Cy$_2$P(*t*-Bu)) was found to have any spectroscopically observable equilibrium between L_2Ni and L_1Ni (1:4 L_2:L_1), with a %V_{bur} (*min*) value of 32.0% near the speciation cutoff. Using Cy$_2$P(*t*-Bu) as a reference, the free energy of ligand dissociation (ΔG_{dissoc}) was calculated for 20 L_2Ni(benzaldehyde) complexes using DFT (Figure 4C). A %V_{bur} (*min*) cutoff of 32% cleanly separated the regions of positive and negative ΔG_{dissoc}, with the remote steric bulk of the DinoPhos ligands and DrewPhos having minimal impacts on dissociation energy. Furthermore, the sharp downtick in the ΔG_{dissoc} values as the %V_{bur} (*min*) of the phosphine approached 32% corresponded with a significant uptick in the Ni–P bond length of the computed L_2 complex, a reflection of the increased steric pressure caused by filling

Ni's first coordination sphere at this value. Together, these studies demonstrate the strong physical significance of the $\%V_{bur}$ (*min*) parameter and the 32% threshold value observed experimentally in the datasets.

Development of threshold analysis algorithm. With the identification of sharp reactivity cliffs in Ni SMC datasets, we sought to formalize the analysis to aid in the automated discovery of thresholds and consequent classification of ligands within a diverse array of reaction datasets. While $\%V_{bur}$ (*min*) was the most successful parameter in classifying ligands in the Ni-catalyzed cross-coupling reactions, the workflow was designed to use all available parameters, and was implemented as follows: the user first defines the % yield or selectivity for a "successful" reaction (either above "ligand-less" control reactivity or a single catalyst turnover), after which the data is parsed by a single-node decision tree algorithm equipped with any descriptor sets provided to it. The algorithm then determines the location of the threshold (if present) for each feature (see SI for details). A consequence of this analysis is the dissection of datasets into four sectors of a confusion matrix: 1) *active* ligands that *meet* the threshold speciation criterion (true positives), 2) *inactive* ligands that correctly *do not meet* the criterion (true negatives), 3) *active* ligands that *do not meet* the criterion (false negatives), and 4) *inactive* ligands that *meet* the criterion but fail for other reasons (false positives) (*37*). These groupings can then in theory be analyzed further using statistical modeling or as targets for mechanistic interrogation (*38*).

Applying this workflow to the Ni datasets, we were able to evaluate the algorithm's ability to computationally identify and quantify the thresholds observed empirically at the outset (see SI for details). Most of the false positives in the classifications were ligands that were either electron-poor or contained catalyst-poisoning functionality, and thus failed for reasons other than

speciation. As an example, P(4-CF_3Ph)$_3$ was found to form L_2Ni(4-fluorobenzaldehyde) complexes but was inactive in all of the catalytic reactions.

Threshold analysis in Pd-catalyzed cross-coupling reactions. Considering the success of the classification tool for Ni-catalyzed cross-coupling reactions, we sought to determine if %V_{bur} (*min*) could also be applied in identifying speciation more broadly. In particular, we investigated various Pd-catalyzed cross-coupling reactions wherein the formation of L_1Pd versus L_2Pd species has been demonstrated to be a key facet of determining reaction outcome (*27, 39*). In one case study, we probed a Pd-catalyzed SMC of aryl triflates, for which L_2Pd is proposed to be necessary for C–O bond oxidative addition (**VII**, Figure 5A) (*27, 40*). The reliance on L_2Pd in catalysis also provided an opportunity to test the DinoPhos ligands for the first time in Pd-catalysis. We generated a dataset using 56 phosphines and found a %V_{bur} (*min*) reactivity threshold at 32.4% (**VII**, Figure 5B). The reactivity cliff mirrored those of the Ni systems in both the cutoff value and directionality of active/inactive regions. Further, DrewPhos and CyTyrannoPhos were both correctly classified as active ligands based on their %V_{bur} (*min*) values below the threshold and performed similarly to "undecorated" PPh_3 and $CyPPh_2$, respectively. Spectroscopic studies corroborated these results, with the detection of L_2Pd(dba) by ^{31}P NMR for DrewPhos and the DinoPhos ligands studied, including less active CyTriceraPhos (see SI for details). A necessity of the analysis for reaction **VII** was to partition and classify Buchwald-type phosphines separately, regardless of %V_{bur} (*min*) (see SI). This is likely due to the fact that they can occupy two coordination sites, a design element of these ligands that allows them to mimic an L_2Pd species during catalysis through stabilizing Pd-arene interactions (*24, 40, 41*). Consistent with previous investigations by the Sigman lab into the chemoselectivity of aryl triflate SMCs (*40*), P(*o*-Tol)$_3$ was an outlier in the reaction, despite likely favoring L_1Pd species under the reaction conditions (*42*).

In the next set of case studies, various reactions where L_1Pd species are implicated were evaluated with the classification workflow. We generated datasets for two Pd-catalyzed SMC couplings (**VIII** & **IX**, Figure 5A) with aryl halides, including one reaction with sterically hindered coupling partners, as well as a dataset for a Buchwald-Hartwig amination (**X**, Figure 5A**)**. For the two SMCs, the classification tool revealed a threshold at approximately 29% V_{bur} (*min*), with the active region occurring above that value, indicating that larger ligands—as defined by %V_{bur} (*min*)—are required for effective catalysis (**VIII** & **IX**, Figure 5B). Notably, when comparing reactions **VII** and **VIII,** the opposite directionalities of the observed thresholds are consistent with the extensive literature precedent studying the effects of ligation state on the chemoselectivity of aryl triflate vs. aryl chloride bond activation (*27, 39, 40*). The presence of steric bulk on both coupling partners in reaction **IX** did not significantly impact the value at which the threshold occurred, analogous to what was observed for a sterically hindered nucleophile in reaction **III** of the Ni-catalyzed datasets. Perhaps the most striking example is that of the Buchwald-Hartwig amination (**X**, Figure 5B) with a clear reactivity cliff between high yielding reactions and those with 0% yield at and below 31% V_{bur} (*min*). Two datasets mined from the literature were also evaluated: a stereospecific Pd-catalyzed SMC previously studied by Biscoe, Sigman and coworkers (*18*) (**XI**, Figure 5A) and a Heck reaction reported by Hartwig and coworkers (*43*) (**XII**, Figure 5A). In both cases, %V_{bur} (*min*) thresholds were observed and suggest that L_1Pd species are responsible for catalysis (**XI** & **XII**, Figure 5B).

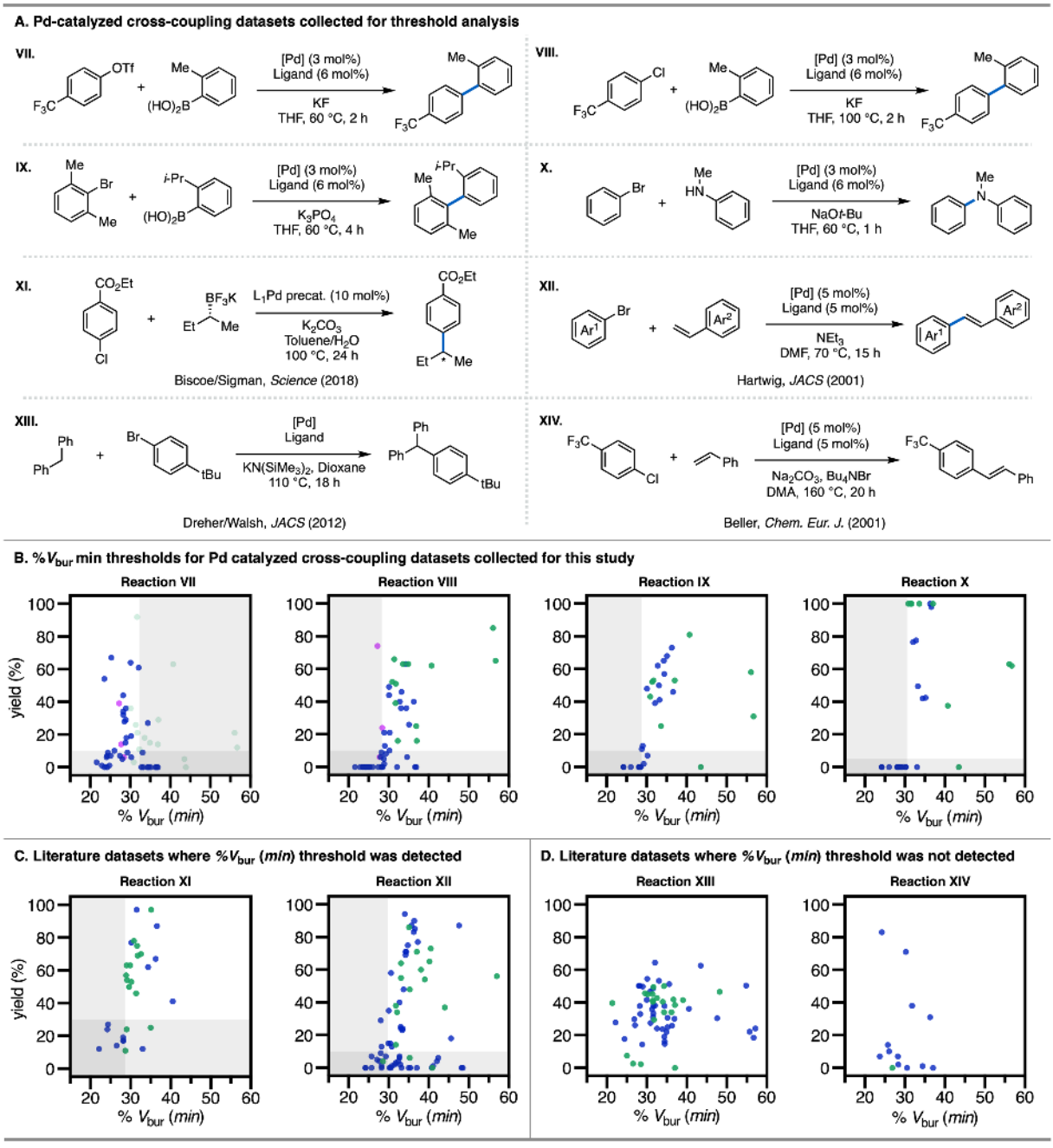

Fig. 5. Threshold analysis for Pd-catalyzed cross-coupling reactions. (**A**) Reaction schemes for reactions analyzed. **VII-X** collected for this study (see SI for exact reaction conditions), **XI**(*18*), **XII** (*43*), **XIII**(*44*), and **XIV**(*45*) mined from literature sources. (**B**) Threshold analysis of Pd datasets **VII-X**. (**C**) Threshold analysis of literature Pd datasets **XI-XII.** (**D**) Threshold analysis of literature Pd datasets **XIII-XIV**, where no %V_{bur} (*min*) threshold is present. For all plots, pink dots = DinoPhos-type ligands, green dots = Buchwald-type ligands, blue dots = all others.

We recognized that there are circumstances where ligand steric properties may not have as significant of an impact on the reaction outcome, and thus a threshold would not be expected. In

our literature mining efforts, we identified two datasets where no phosphine steric threshold was found: a Pd-catalyzed Csp^3-H arylation reported by Dreher, Walsh and coworkers (*44*) (**XIII**, Figure 5) and a Pd-catalyzed Heck cross-coupling studied by Beller and coworkers (*45*) (**XIV**, Figure 5). Possible explanations for these examples include high levels of ligandless background reactivity and/or catalytic cycles that are less sensitive to ligation state, possibly due to the generation of catalytically-active Pd nanoparticles (*46, 47*). The ability to rapidly identify these scenarios in datasets can serve as a valuable mechanistic probe given the physical importance of $\%V_{bur}$ (*min*) (*vide supra*).

Summary and Outlook: The threshold values and directionality found for each of the datasets studied in this work are summarized in Fig. 6. Comparing the Ni- and Pd-catalyzed reactions reveals several mechanistically interesting features about Ni and Pd catalysis, as well as phosphine steric effects more generally. First, the opposite threshold directionalities of the Ni- and Pd-catalyzed Suzuki–Miyaura coupling reactions of aryl halides (II-V, IX, VIII) point to clear differences in mechanistic requirements between the two metals with regard to speciation for this reaction (*48*). Thus, the classification workflow provides a means to compare the two metals head-to-head and sheds light on the orthogonal ligand design principles often necessary for each metal (*19, 49*). Additionally, despite the differences in

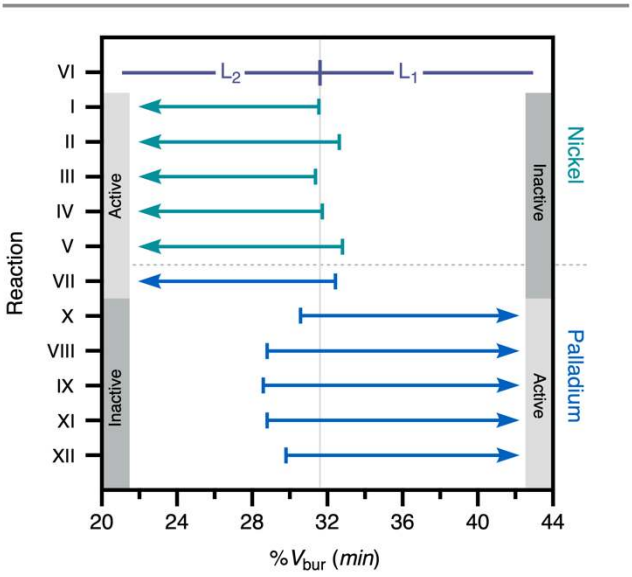

Fig. 6. Summary of reactivity thresholds. $\%V_{bur}$ (*min*) reactivity threshold locations and directionalities for all Ni (**I**–**V** (green)) and Pd (**VII**–**XII** (blue)) catalyzed reactions under study (excluding **XIII** & **VIV** where no threshold was found). The L_1 and L_2 regions defined by the spectroscopic ligation state studies (**VI** (purple)).

coordination sphere size between Ni and Pd, the location of the threshold for the Ni datasets and the Pd datasets with the sharpest reactivity cliffs (**VII** and **X**) occur at approximately the same location of 32% V_{bur} (*min*), linking the catalytic outcome for both metals to ligand-controlled thermodynamic L_1 vs. L_2 propensity.

It is also worth noting that the observed thresholds occurred with different sensitivities and with some variation in value. Indeed, an overlap area can be observed wherein ligands with %V_{bur} (*min*) values between 29% and 32% work in all of the reactions tested with both metals (with the exception of reaction **X**). Accordingly, this may signify a region of %V_{bur} (*min*) values in which L_2M is thermodynamically favored in the resting state but L_1M is still attainable; within this region, the equilibrium between L_2M and L_1M would be impacted by the temperature and concentration of the reaction. This is known to be the case with phosphines such as PCy_3 (*39*), and the decrease in ΔG_{dissoc} between 29% and 32% (Figure 4C) corroborates this hypothesis. Interestingly, even in the data for Ni-catalyzed cross-couplings, the most active ligands generally fell within these limits (Figure 2). This observation suggests that L_1 intermediates and/or transition states may be relevant in Ni catalysis (*50, 51*), but that the ability to attain an L_2 resting state is necessary (*33, 52, 53*), as evidenced by the sharp reactivity cliffs.

In conclusion, we have developed a strategy for the binary classification of monodentate phosphine ligation state and reactivity in cross-coupling catalysis. In searching the feature space of structurally diverse monodentate phosphines, we identified %V_{bur} (*min*) as the parameter capable of bifurcating datasets on the basis of distinct mechanistic outcomes. We envision that this easily adopted tool should facilitate mechanistic studies of related organometallic reactions and enable reaction development through prediction of active/inactive and mono/bis-ligating phosphines prior to synthesis. While we recognize %V_{bur} (*min*) will not capture reactivity trends

across all phosphines, the ability to identify outliers (especially false negatives) in the analysis can motivate the development of new parameters and targeted mechanistic study. Taken together, this study highlights how classification analysis can serve as an important mechanistic and predictive tool, complementary to LFERs, to facilitate statistical modeling of reactivity cliffs in chemistry.

References:

1. L. P. Hammett, The Effect of Structure upon the Reactions of Organic Compounds. Benzene Derivatives. *Journal of the American Chemical Society* **59**, 96-103 (1937).

2. P. R. Wells, Linear Free Energy Relationships. *Chemical Reviews* **63**, 171-219 (1963).

3. E. N. Jacobsen, W. Zhang, M. L. Guler, Electronic tuning of asymmetric catalysts. *Journal of the American Chemical Society* **113**, 6703-6704 (1991).

4. J. O. Schreck, Nonlinear Hammett relationships. *J. Chem. Ed.* **48**, 103 (1971).

5. C. B. Santiago, J. Y. Guo, M. S. Sigman, Predictive and mechanistic multivariate linear regression models for reaction development. *Chem Sci* **9**, 2398-2412 (2018).

6. N. A. Romero, D. A. Nicewicz, Organic Photoredox Catalysis. *Chemical Reviews* **116**, 10075-10166 (2016).

7. D. G. Brown, J. Boström, Analysis of Past and Present Synthetic Methodologies on Medicinal Chemistry: Where Have All the New Reactions Gone? *J Med Chem* **59**, 4443-4458 (2016).

8. S. Xu, E. H. Kim, A. Wei, E.-i. Negishi, Pd- and Ni-catalyzed cross-coupling reactions in the synthesis of organic electronic materials. *Science and Technology of Advanced Materials* **15**, 044201 (2014).

9. J. F. Hartwig, *Organotransition Metal Chemistry: From Bonding to Catalysis*. (University Science Books, 2010).

10. C. C. C. Johansson Seechurn, M. O. Kitching, T. J. Colacot, V. Snieckus, Palladium-Catalyzed Cross-Coupling: A Historical Contextual Perspective to the 2010 Nobel Prize. *Angewandte Chemie International Edition* **51**, 5062-5085 (2012).

11. D. J. Durand, N. Fey, Computational Ligand Descriptors for Catalyst Design. *Chem Rev* **119**, 6561-6594 (2019).

12. C. A. Tolman, Phosphorus ligand exchange equilibriums on zerovalent nickel. Dominant role for steric effects. *J. Am. Chem. Soc.* **92**, 2956-2965 (1970).

13. C. A. Tolman, Steric effects of phosphorus ligands in organometallic chemistry and homogeneous catalysis. *Chem. Rev.* **77**, 313-348 (1977).

14. D. White, B. C. Tavener, P. G. L. Leach, N. J. Coville, Solid angles I. The radial profile. *Journal of Organometallic Chemistry* **478**, 205-211 (1994).

15. K. C. Harper, E. N. Bess, M. S. Sigman, Multidimensional steric parameters in the analysis of asymmetric catalytic reactions. *Nat Chem* **4**, 366-374 (2012).

16. A. Poater *et al.*, SambVca: A Web Application for the Calculation of the Buried Volume of N-Heterocyclic Carbene Ligands. *European Journal of Inorganic Chemistry* **2009**, 1759-1766 (2009).

17. H. Clavier, S. P. Nolan, Percent buried volume for phosphine and N-heterocyclic carbene ligands: steric properties in organometallic chemistry. *Chem Commun (Camb)* **46**, 841-861 (2010).

18. S. Zhao *et al.*, Enantiodivergent Pd-catalyzed C–C bond formation enabled through ligand parameterization. *Science* **362**, 670 (2018).

19. K. Wu, A. G. Doyle, Parameterization of phosphine ligands demonstrates enhancement of nickel catalysis via remote steric effects. *Nat Chem* **9**, 779-784 (2017).

20. H. Y. Liu, K. Eriks, A. Prock, W. P. Giering, Quantitative analysis of ligand effects (QALE). Systematic study of iron-phosphorus bond lengths and their relationship to steric thresholds. *Organometallics* **9**, 1758-1766 (1990).

21. T. Gensch *et al.*, A comprehensive discovery platform for organophosphorus ligands for catalysis. *ChemRxiv*, (2021).

22. H. Clavier, S. P. Nolan, Percent buried volume for phosphine and N-heterocyclic carbene ligands: steric properties in organometallic chemistry. *Chem. Comm.* **46**, 841-861 (2010).

23. F. Barrios-Landeros, B. P. Carrow, J. F. Hartwig, Effect of ligand steric properties and halide identity on the mechanism for oxidative addition of haloarenes to trialkylphosphine Pd(0) complexes. *J Am Chem Soc* **131**, 8141-8154 (2009).

24. R. Martin, S. L. Buchwald, Palladium-Catalyzed Suzuki−Miyaura Cross-Coupling Reactions Employing Dialkylbiaryl Phosphine Ligands. *Accounts of Chemical Research* **41**, 1461-1473 (2008).

25. A. A. Thomas, A. F. Zahrt, C. P. Delaney, S. E. Denmark, Elucidating the Role of the Boronic Esters in the Suzuki–Miyaura Reaction: Structural, Kinetic, and Computational Investigations. *Journal of the American Chemical Society* **140**, 4401-4416 (2018).

26. G. C. Fu, The development of versatile methods for palladium-catalyzed coupling reactions of aryl electrophiles through the use of P(t-Bu)3 and PCy3 as ligands. *Acc Chem Res* **41**, 1555-1564 (2008).

27. F. Schoenebeck, K. N. Houk, Ligand-controlled regioselectivity in palladium-catalyzed cross coupling reactions. *J Am Chem Soc* **132**, 2496-2497 (2010).

28. F.-S. Han, Transition-metal-catalyzed Suzuki–Miyaura cross-coupling reactions: a remarkable advance from palladium to nickel catalysts. *Chemical Society Reviews* **42**, 5270-5298 (2013).

29. A. P. Cinderella, B. Vulovic, D. A. Watson, Palladium-Catalyzed Cross-Coupling of Silyl Electrophiles with Alkylzinc Halides: A Silyl-Negishi Reaction. *J Am Chem Soc* **139**, 7741-7744 (2017).

30. Cone angle values used in text are those for the Boltzmann weighted average of the conformational ensemble from the descriptor library. Minimum cone angles were also evaluated but for simplicity are shown in the SI.

31. A. J. Kendall, L. N. Zakharov, D. R. Tyler, Steric and Electronic Influences of Buchwald-Type Alkyl-JohnPhos Ligands. *Inorg Chem* **55**, 3079-3090 (2016).

32. Buchwald-type phosphines are known to act as structurally bidentate-like ligands with Pd due to stabilizing interactions between the arene and the metal. While little is currently known about the structural behavior of these ligands with Ni, this semi-bidentate binding may enable certain Ni-catalyzed reactions to occur despite only one phosphine bound; their mode of action in these case studies is the subject of ongoing investigation..

33. E. A. Standley, S. J. Smith, P. Müller, T. F. Jamison, A Broadly Applicable Strategy for Entry into Homogeneous Nickel(0) Catalysts from Air-Stable Nickel(II) Complexes. *Organometallics* **33**, 2012-2018 (2014).

34. D. Walther, Reaktionen von heteroolefinen an zentralmetallen in niedrigen oxidationsstufen: stabile aldehydkomplexe des nickel(O) und verwandte verbindungen. *Journal of Organometallic Chemistry* **190**, 393-401 (1980).

35. M. Ohashi, H. Saijo, T. Arai, S. Ogoshi, Nickel(0)-Catalyzed Formation of Oxaaluminacyclopentenes via an Oxanickelacyclopentene Key Intermediate: Me2AlOTf-Assisted Oxidative Cyclization of an Aldehyde and an Alkyne with Nickel(0). *Organometallics* **29**, 6534-6540 (2010).

36. I. A. Guzei, M. Wendt, An improved method for the computation of ligand steric effects based on solid angles. *Dalton Transactions*, 3991-3999 (2006).

37. Given that other ligand features can and will lead to poor catalyst performance, the presence of false positives should not be viewed as detrimental to the success/accuracy of the classifier.

38. Z. L. Niemeyer *et al.*, Parameterization of Acyclic Diaminocarbene Ligands Applied to a Gold(I)-Catalyzed Enantioselective Tandem Rearrangement/Cyclization. *Journal of the American Chemical Society* **139**, 12943-12946 (2017).

447 39. A. F. Littke, C. Dai, G. C. Fu, Versatile Catalysts for the Suzuki Cross-Coupling of
448 Arylboronic Acids with Aryl and Vinyl Halides and Triflates under Mild Conditions. *Journal of*
449 *the American Chemical Society* **122**, 4020-4028 (2000).

450 40. Z. L. Niemeyer, A. Milo, D. P. Hickey, M. S. Sigman, Parameterization of phosphine
451 ligands reveals mechanistic pathways and predicts reaction outcomes. *Nat Chem* **8**, 610-617
452 (2016).

453 41. K. L. Billingsley, K. W. Anderson, S. L. Buchwald, A Highly Active Catalyst for Suzuki–
454 Miyaura Cross-Coupling Reactions of Heteroaryl Compounds. *Angewandte Chemie International*
455 *Edition* **45**, 3484-3488 (2006).

456 42. J. F. Hartwig, F. Paul, Oxidative Addition of Aryl Bromide after Dissociation of Phosphine
457 from a Two-Coordinate Palladium(0) Complex, Bis(tri-o-tolylphosphine)Palladium(0). *Journal of*
458 *the American Chemical Society* **117**, 5373-5374 (1995).

459 43. J. P. Stambuli, S. R. Stauffer, K. H. Shaughnessy, J. F. Hartwig, Screening of
460 Homogeneous Catalysts by Fluorescence Resonance Energy Transfer. Identification of Catalysts
461 for Room-Temperature Heck Reactions. *Journal of the American Chemical Society* **123**, 2677-
462 2678 (2001).

463 44. J. Zhang, A. Bellomo, A. D. Creamer, S. D. Dreher, P. J. Walsh, Palladium-Catalyzed
464 C(sp3)–H Arylation of Diarylmethanes at Room Temperature: Synthesis of Triarylmethanes via
465 Deprotonative-Cross-Coupling Processes. *Journal of the American Chemical Society* **134**, 13765-
466 13772 (2012).

467 45. A. Zapf, M. Beller, Palladium Catalyst Systems for Cross-Coupling Reactions of Aryl
468 Chlorides and Olefins. *Chemistry – A European Journal* **7**, 2908-2915 (2001).

469 46. S. S. Zalesskiy, V. P. Ananikov, Pd2(dba)3 as a Precursor of Soluble Metal Complexes
470 and Nanoparticles: Determination of Palladium Active Species for Catalysis and Synthesis.
471 *Organometallics* **31**, 2302-2309 (2012).

472 47. N. W. J. Scott *et al.*, The ubiquitous cross-coupling catalyst system 'Pd(OAc)2'/2PPh3
473 forms a unique dinuclear PdI complex: an important entry point into catalytically competent cyclic
474 Pd3 clusters. *Chemical Science* **10**, 7898-7906 (2019).

475 48. S. Z. Tasker, E. A. Standley, T. F. Jamison, Recent advances in homogeneous nickel
476 catalysis. *Nature* **509**, 299-309 (2014).

477 49. C. M. Lavoie, M. Stradiotto, Bisphosphines: A Prominent Ancillary Ligand Class for
478 Application in Nickel-Catalyzed C–N Cross-Coupling. *ACS Catalysis* **8**, 7228-7250 (2018).

479 50. H. Shirataki, M. Ohashi, S. Ogoshi, Nickel-Catalyzed Three-Component Coupling
480 Reaction of Tetrafluoroethylene and Aldehydes with Silanes via Oxa-Nickelacycles. *European*
481 *Journal of Organic Chemistry* **2019**, 1883-1887 (2019).

51. We recognize that there are some instances where Ni will be L_1 throughout the catalytic cycle allowing ligands like P(*t*-Bu)$_3$ to be employed successfully. See ref (50).

52. N. Hazari, P. R. Melvin, M. M. Beromi, Well-defined nickel and palladium precatalysts for cross-coupling. *Nat Rev Chem* **1**, (2017).

53. P.-A. Payard, L. A. Perego, I. Ciofini, L. Grimaud, Taming Nickel-Catalyzed Suzuki-Miyaura Coupling: A Mechanistic Focus on Boron-to-Nickel Transmetalation. *ACS Catalysis* **8**, 4812-4823 (2018).

Acknowledgements: The authors thank Dr. Phil Jeffrey for assistance with X-Ray structure determination and Dr. Kevin Wu for helpful discussions and directions. Additionally, we thank Prof. F. Dean Toste for helpful discussions related to the preparation of the manuscript.

Funding: NSF CCI Center for Computer Assisted Synthesis (CHE-1925607)

Author Contributions: T.G., M.S.S., and A.G.D. conceived the project. S.H.N.-S., S.R.S., J.E.B., and H.C.J. performed the experiments and analyzed the data. E.P., T.G., and S.R.S. developed the classification algorithm. M.S.S. and A.G.D. oversaw the project. S.H.N.-S., J.E.B., S.R.S., M.S.S., and A.G.D. wrote the manuscript with contributions from all authors.

Competing Interests: The authors declare no competing interests.

Data and Materials Availability: X-ray crystallographic data are available free of charge from the Cambridge Crystallographic Data Centre, under reference numbers 2069892-2069895. Coordinates of all computed structures are included in a separate zip file. All other experimental, computational, spectroscopic, and crystallographic data are included in the supplementary materials. The code used in this project is available at https://github.com/SigmanGroup/Threshold.

Supplementary Materials

Materials and Methods
Figs. S1 to S116
Tables S1 to S18
References